The Astrophysical Journal Letters, 801:L2 (7pp), 2015 March 1 doi:10.1088/2041-8205/801/1/L2

FLOWS AND WAVES IN BRAIDED SOLAR CORONAL MAGNETIC STRUCTURES

V. Pant[1], A. Datta[1,2], and D. Banerjee[1,3]
[1] Indian Institute of Astrophysics, Bangalore 560 034, India; vaibhav@iiap.res.in
[2] HKBK College of Engineering, Bangalore 560045, India
[3] Center of Excellence in Space Sciences, IISER Kolkata, India
Received 2014 November 24; accepted 2015 January 25; published 2015 February 24

ABSTRACT

We study the high frequency dynamics in the braided magnetic structure of an active region (AR 11520) moss as observed by the High-Resolution Coronal Imager (Hi-C). We detect quasi-periodic flows and waves in these structures. We search for high frequency dynamics while looking at power maps of the observed region. We find that shorter periodicities (30–60 s) are associated with small spatial scales which can be resolved by Hi-C only. We detect quasi-periodic flows with a wide range of velocities, from 13–185 km s^{-1}, associated with braided regions. This can be interpreted as plasma outflows from reconnection sites. We also find short period and large amplitude transverse oscillations associated with the braided magnetic region. Such oscillations could be triggered by reconnection or such oscillations may trigger reconnection.

Key words: Sun: corona – Sun: oscillations – Sun: UV radiation

Supporting material: animation

1. INTRODUCTION

Understanding the heating mechanism/s of the solar corona is one of the main challenges in solar physics. Two types of mechanisms are widely accepted, namely, impulsive heating by nanoflares (Parker 1988) and wave heating by dissipation of waves.

The High Resolution Coronal Imager (Hi-C; Kobayashi et al. 2014) provided unprecedented details of the active region moss at small spatial scales. It has a diffraction-limited spatial resolution of 0.″3 and cadence of ∼5.5 s. Hi-C has revealed many new features of the corona at small spatial scales (Morton & McLaughlin 2013; Peter et al. 2013; Winebarger et al. 2014). Antiochos et al. (2003) reported a weak intensity variation of ∼10% in the active region moss over a period of hours using *TRACE*. They rule out the possibility of impulsive heating and also conjectured that high-frequency heating could be the source of the observed variability. Brooks & Warren (2009) confirmed the findings of Antiochos et al. (2003) using *Hinode* EIS observation. They did not find strong flows and short term variability in the moss region and concluded that heating is quasi-steady. The high temporal and spatial resolution of Hi-C gave new insight in understanding the mechanism of coronal nanoflare heating. Winebarger et al. (2013) studied inter-moss loops using Hi-C and reported that these cool and dense loops are the result of impulsive heating of magnitude similar to that of coronal nanoflares. Testa et al. (2013) have reported the variability of ∼15–20 s in the active moss region at the foot points of bright hot coronal loops and attributed these to be the signature of impulsive nanoflare events. Hi-C observations have revealed small scale brightening in EUV of duration 25 s and of length scale 0.68 Mm (Régnier et al. 2014). Cirtain et al. (2013) have reported the first evidence of magnetic field braiding and axial twist from Hi-C observations. They have estimated the free energy available to be $\sim 10^{29}$ ergs. The release of this energy due to magnetic reconnection can heat up the loop. A nonlinear force-free field reconstruction of magnetic field lines corresponding to the same field of view (FOV) of Hi-C reveals the braiding and twisting of magnetic fields (Thalmann et al. 2014). They estimated ∼100 times more free energy than estimated by Cirtain et al. (2013). Recently, Tiwari et al. (2014) observed a subflare event at this region just after the Hi-C observations from different channels of the Atmosphearic Imaging Assembly (AIA) on board the Solar Dynamic Observatory (SDO).

Transverse oscillations in the corona have been reported by Tomczyk et al. (2007) using Coronal Multi channel Polarimeter data and by McIntosh et al. (2011) using AIA on SDO. They have reported the typical velocity amplitude of ∼5 km s^{-1}. After the advent of Hi-C Morton & McLaughlin (2013, 2014) reported transverse waves in active region moss with velocity amplitude as high as 11 km s^{-1} and mean periodicity of ∼50 s. They have estimated that about 15% of wave energy is carried to the transition region from the chromosphere.

In this letter we focus on the high frequency dynamics of the active region moss and braided magnetic region as seen from Hi-C, with particular emphasis on the reconnection sites. Recurrent reconnections and waves both can contribute significantly to the heating. We search for the presence of flows, which can be attributed to be the signature of reconnection within the braided magnetic region.

2. OBSERVATIONS AND DATA ANALYSIS

Hi-C took high-resolution images of the solar corona in the Fe XII 193 Å passband. The observations were performed on 2012 July 11 at 18:52:09 UT with the cadence of ∼5.5 s and pixel resolution of ∼0.″103 $pixel^{-1}$ for a duration of 200 s. We used the level 1.5, 4K X 4K data set. This data set is corrected for pointing drift, spacecraft jitter, and atmospheric absorption (Kobayashi et al. 2014). We align the datacube using cross correlation to remove residual drifts and to achieve sub-pixel accuracy (Morton & McLaughlin 2013, 2014).

We also use simultaneous imaging data as recorded by AIA/SDO with EUV narrow band (∼0.″6 $pixel^{-1}$, 12 s cadence). Figure 1(a) shows the AIA 193 Å full disk image. The small black rectangle shows the full Hi-C FOV. Figures 1(b) and (d) show the zoomed-in view of the region marked with the black rectangle in Figure 1(a) as seen in AIA and Hi-C, respectively.

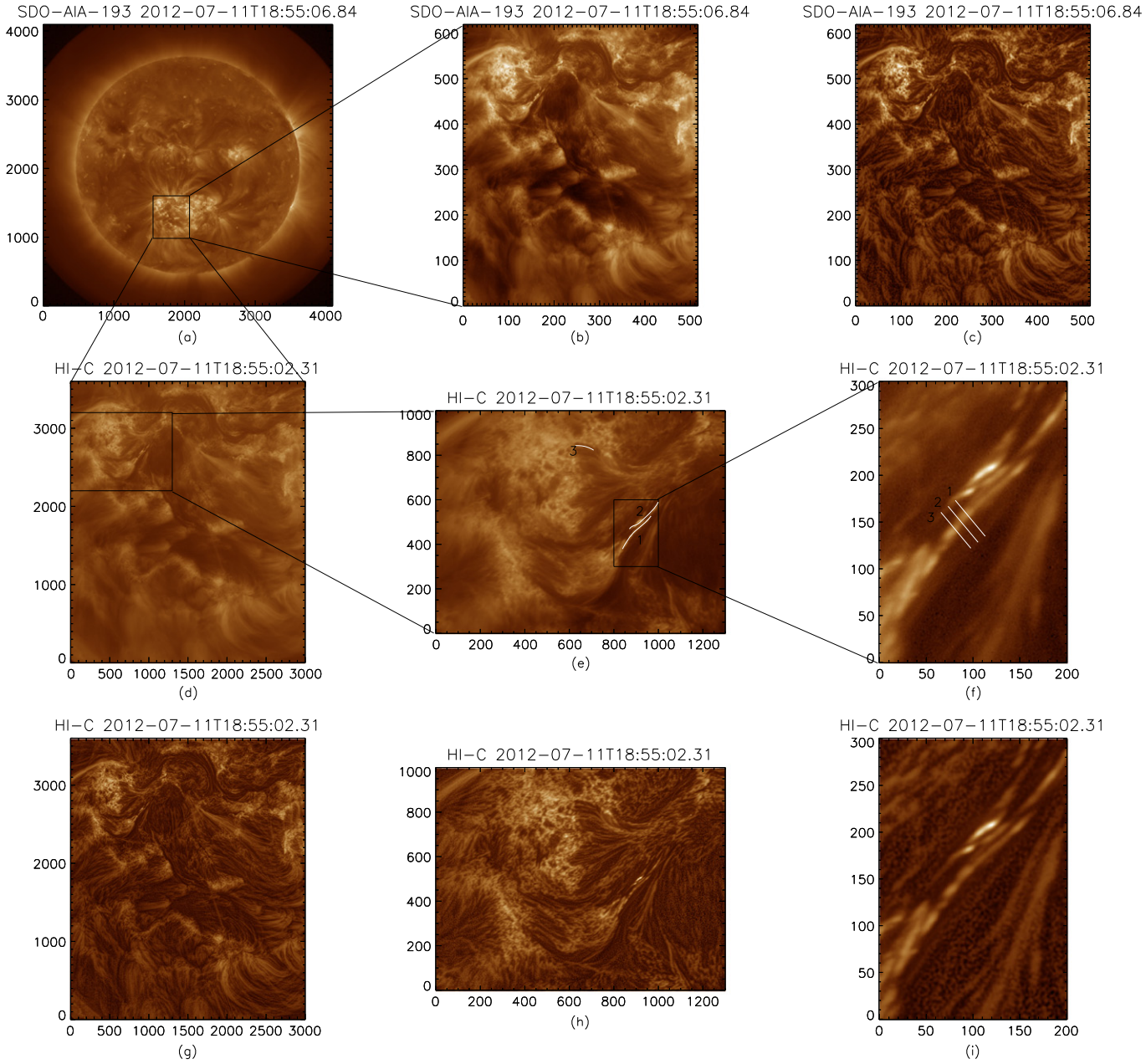

Figure 1. Top panels: (a) AIA 193 Å full disk image. Black rectangle represents the full Hi-C FOV. (b) AIA 193 Å with the same FOV as Hi-C. (c) Reconstructed image, using the multi-Gaussian normalized filter, with the same FOV as shown in (b). Middle Panels: (d) Full FOV of HI-C image. Region under consideration is indicated with the black rectangle. (e) Three curved slits positions, which are used for time–distance maps, indicated by the white curves, are shown. (f) Three slits are placed perpendicular to the threads as indicated by the white lines for the detection of transverse motions. Bottom panel: Reconstructed images, using the multi-Gaussian normalized filter, with the same FOV as shown in the middle panel.

(An animation of this figure is available.)

The black rectangle in Figure 1(d) marks the region of interest (ROI) for further analysis. Figure 1(e) shows the zoomed-in view of the ROI and the curved white slices used for creating time–distance maps. Figure 1(f) shows the zoomed-in view of the subfield of the ROI as marked in Figure 1(e). Due to high noise in the Hi-C images we filter each image into high and low spatial frequency components. The high frequency image shows significant small scale structures; therefore, we filter the high frequency component further. We iterate it up to three times and the resulting high frequency image contains only uncorrelated noise. Finally, we subtract the high frequency image from the original image. Furthermore, in order to bring out structures at different spatial scales, we use a normalized multi-Gaussian filter (Morgan and Druckmüller 2014) to high frequency filtered images. We choose the width of Gaussian filter to be 11, 21, 41, and 81 pixels for the ROI and 21, 41, 101, 201, and 1001 pixels for the Hi-C full FOV. We add Gaussian-filtered images of different spatial scales with equal weight to obtain a single multi-Gaussian filtered image. The above procedure is repeated for the AIA 193 Å image with the width of the Gaussian filter being 11, 21, 41, and 81 pixels; the filtered image is shown in Figure 1(c). The filtered images of the corresponding images of Hi-C in Figure 1 (middle panel) are shown in the bottom panel of Figure 1. An animation is

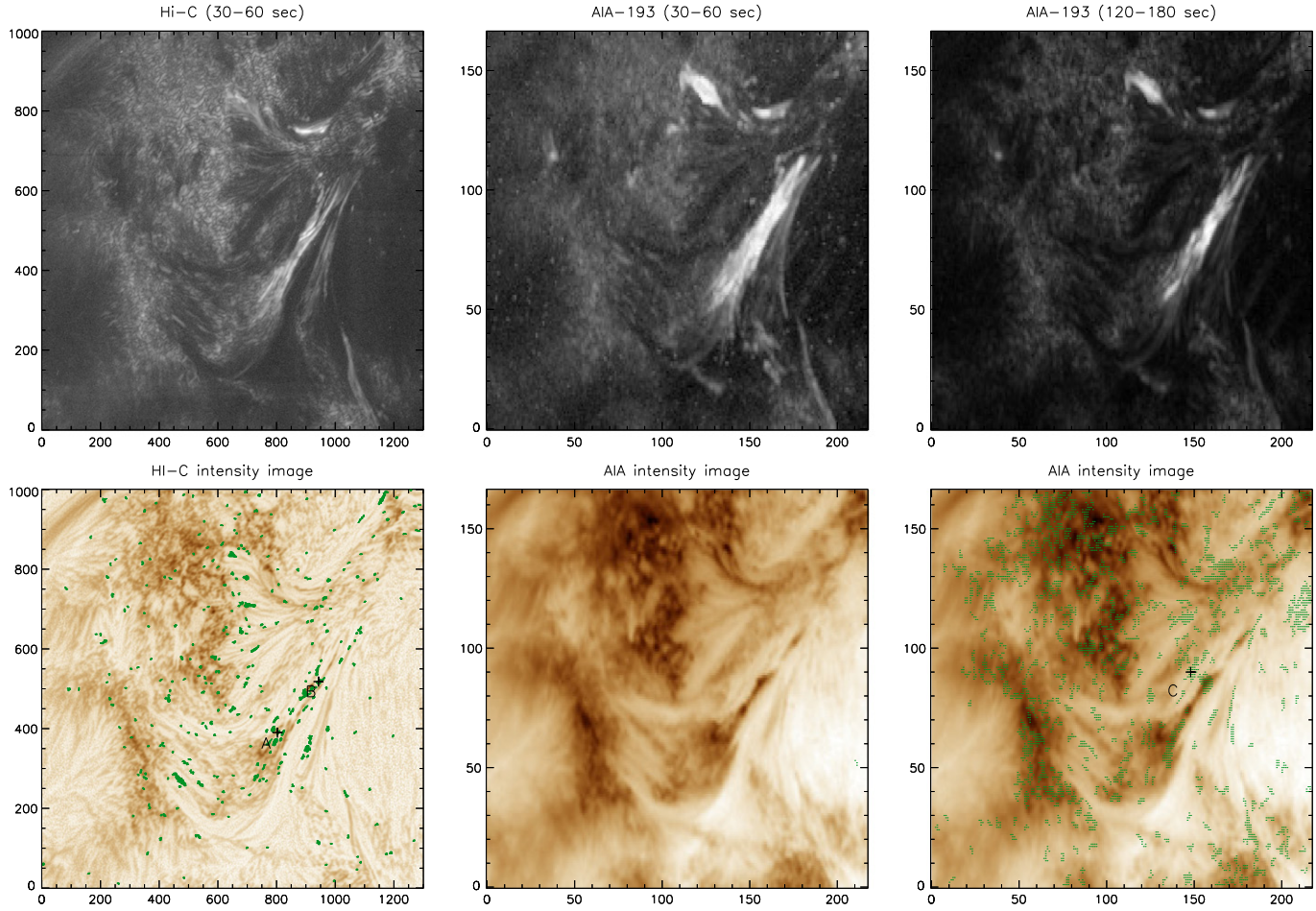

Figure 2. Top panels: (Left) Power map of the Hi-C ROI plotted in logarithmic scale for 30–60 s. (Middle) Power map of the AIA 193 Å ROI plotted in logarithmic scale for 30–60 s periods. (Right) Power map of AIA 193 Å ROI plotted in logarithmic scale for 120–180 s. Bottom panel: (Left) Filtered inverted intensity image of Hi-C overplotted with pixel positions having significant power greater than 95% confidence level in green. (Middle and right) Inverted intensity image of AIA 193 Å overplotted with pixel positions with significant power greater than 95% confidence level in green.

available. The left panel in the animation corresponds to the Hi-C original intensity images while the right panel corresponds to the multi-Gaussian filtered images.

3. RESULTS

We will focus on the distribution of power as calculated from wavelet methods to identify the locations where the high frequency dynamics are present.

3.1. Power and Wavelet Maps

We perform wavelet analysis at each pixel location of Hi-C ROI and corresponding FOV of AIA 193 Å . Figure 2, top left panel, shows the power map of the Hi-C ROI in the 30–60 s interval and the filtered image of Hi-C overplotted with the pixel positions marked in green where the global significance level of power is greater than 95% confidence level (Torrence & Compo 1998) for a white noise process (see Figure 2 bottom left panel). We limit ourselves to the 30–60 s interval because we note that for higher frequencies (15–30 s), the wavelet starts picking up noise and it is difficult to distinguish between noise and true signal variation. To limit the noise we discard isolated pixel locations and set the threshold as 9 pixels on the size of the detected regions over the global significance level. We carry out a similar analysis for AIA 193 Å. The cadence of AIA is low (12 s) compared to Hi-C (5.4 s) thus there will be fewer data points due to the finite duration of the time series. Therefore we choose a longer time series of 10 minutes starting from 18:50:00 UT to 18:60:00 UT for AIA 193 Å. We find that even after choosing a longer time series, significant power in shorter periodicities (30–60 s) is absent in the AIA FOV (Figure 2, bottom middle panel) while significant power is present in longer periodicities (120–180 s) as shown in Figure 2, bottom right panel. For AIA we set the threshold as two pixels on the size of the detected regions over the global significance level.

Wavelet maps of pixel locations marked as A and B in Hi-C FOV (see Figure 2 bottom left panel) are shown in Figures 3(a) and (b), respectively. Figure 3(a), top panel, shows the original Hi-C light curve without any smoothing at the position marked A with error bars. Errors in data points are calculated as $\sqrt{0.23F + 588.4}$ (Morton & McLaughlin 2013), where F is the intensity value at pixel position A. The bottom left panel shows the wavelet result which displays the temporal evolution of different periodicities. Power is plotted in inverted colors, therefore black indicates the region of strongest power. The cross-hatched region is called the cone of influence. This region can suffer from edge effects; therefore, periods observed in this region are not reliable. The bottom right panel is the global wavelet plot, which is the time average of the wavelet plot. The

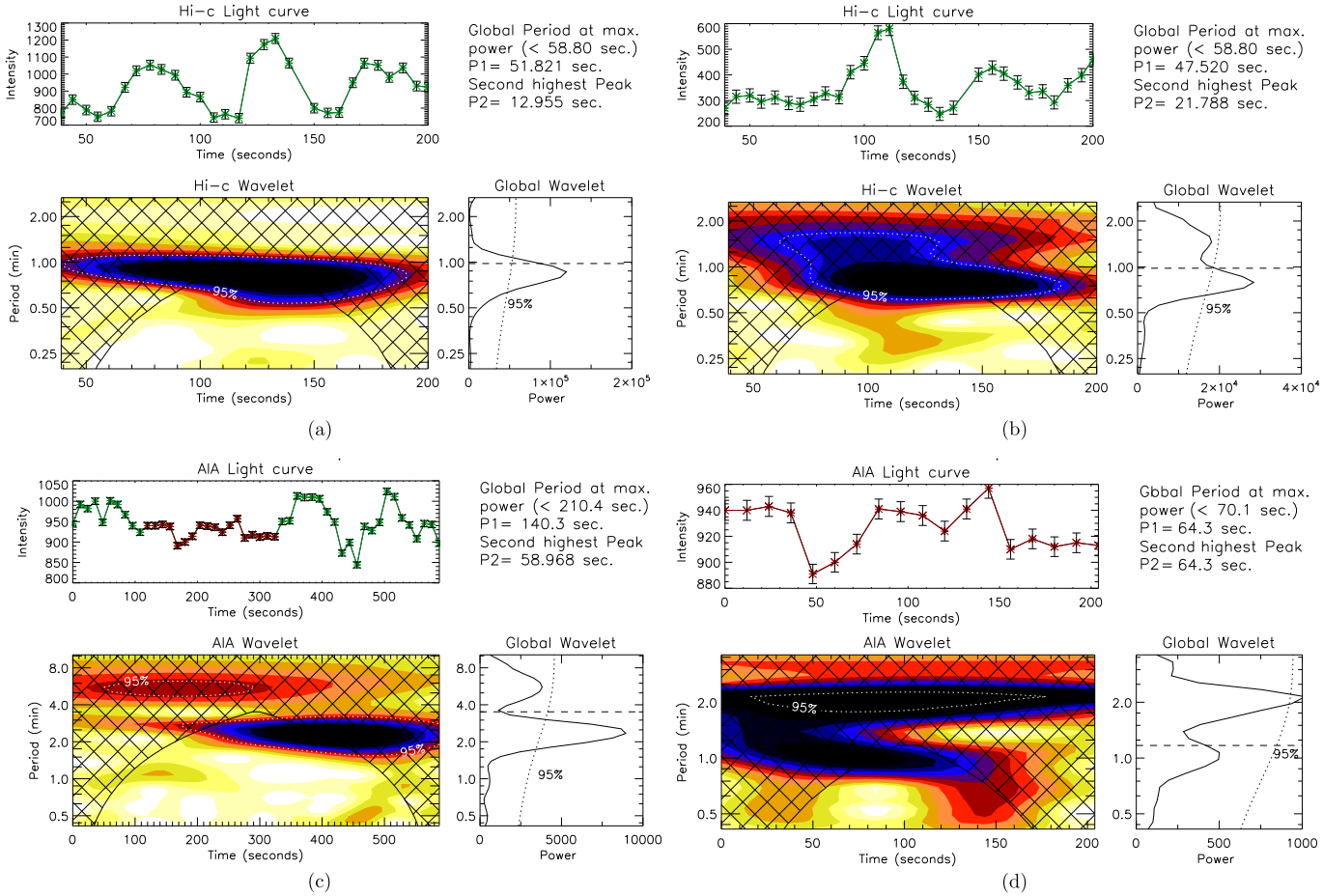

Figure 3. (a) Wavelet map of Hi-C intensity at pixel position "A" marked in Figure 2, bottom left panel. (b) Wavelet map of Hi-C intensity at pixel position "B" marked in Figure 2, bottom left panel. (c) Wavelet map of AIA intensity at pixel position "C" marked in Figure 2, bottom right panel. Data points marked in red are co-temporal with Hi-C duration. (d) Wavelet map of AIA intensity at pixel position "C" marked in Figure 2, bottom right panel, co-temporal with the Hi-C duration.

horizontal dashed line is the cutoff above which edge effects come into play and the dotted line marks the 95% significance level for a white noise process. We find that significant power peaks at ∼52 s followed by a second highest peak at ∼13 s. The second peak is not significant and it could be due to small variations in the light curve that are within the error limits. A similar analysis is repeated for pixel position B where the maximum significant power is at ∼48 s and the second peak is at ∼22 s (see Figure 3(b)). This analysis reveals that there is an indication of periodicities of around 15–30 s but they are not significant. Such periodicities could be the manifestation of small variation of intensities which are within error limits.

Figure 3(c) shows the wavelet map of AIA 193 Å at pixel location marked as C (see Figure 2, bottom right panel). We choose a longer time series of 10 minutes starting from 18:50:00 UT. Figure 3(c), top panel, shows the AIA light curve with error estimates. Errors are calculated as $\sqrt{0.06F + 2.3}$ (Yuan & Nakariakov 2012), where F is the intensity value at a given pixel position. Intensity values marked in red are co-temporal with Hi-C observations. We find that significant power peaks at ∼140 s. However, shorter periodicities are also present as small peaks at ∼59 s and 30 s. To investigate the presence of shorter periodicities below 60 s, we perform wavelet analysis of the pixel location at C for the duration co-temporal with the Hi-C observations as shown in Figure 3(d). We note that periods ∼60 s do exist but they are below the significance level.

It is worthwhile to note that the power map reveals finer structures in the moss and braided magnetic region where power is concentrated. In Figure 2 (bottom left panel) it is evident that significant power (pixels marked in green) within 30–60 s are lying over the active moss and braided magnetic field region in Hi-C FOV while significant power at these periods is absent in AIA 193 Å (Figure 2 (bottom middle panel)). However, significant power at longer periods (120–180 s) are lying over the active moss and braided magnetic field region in AIA FOV (Figure 2 (bottom right panel)). It suggests that shorter periodicities (30–60 s) are present in smaller spatial scales, which cannot be resolved by AIA. Therefore, such short periodicites are almost absent in AIA 193 Å FOV.

3.2. *Quasi-periodic Flows and Transverse Oscillation*

To study the flow within the braided magnetic region, we place three artificial curved slices along some specific threads as marked in Figure 1(e). A two-dimensional time–distance diagram (x–t) corresponding to each of the three slices is created (see Figure 4), where the x axis represents the time in seconds and the yaxis represents the distance along the slit in Mm. The thick black region in x–t map (Figure 4 top panel)

represents the data gap. For ridges where structures can be resolved, a Gaussian curve along the column is fitted and the mean values with one sigma error bars are estimated. The ridge is then fitted with straight line. For extended or faint ridges the Gaussian curve fitting is not feasible thus we fitted them visually with straight line. Figure 4, bottom panel, shows the running difference x–t maps corresponding to maps in Figure 4, top panel.

Several ridges are seen in the x–t maps with different slopes at different times and with different lifetimes as shown in Figure 3. Slopes of the ridges give an estimate of the velocities of the plasma outflow. The plasma outflows are found to be quasi-periodic with a large range of velocities from 13–185 km s^{-1}(see Figure 4) within our ROI, which could be closely associated with reconnection sites.

Due to the high spatial resolution Hi-C also helps us to probe transverse oscillations associated with fine threads. For that we place three transverse slices across one highly braided structure as marked in Figure 1(f). For transverse slices, the method of analysis is the same as what we adopted for curved slices. The x–t map (Figure 5) is fitted with a harmonic curve represented by the formula

$$y = a + b \sin(\omega t + \phi), \quad (1)$$

where a is a constant, b is the amplitude, ω is the frequency, and ϕ is the phase. The amplitude of oscillation is found to be 110 ± 109 km (111 ± 102 km and 67 ± 105 km) and the period of oscillation is found to be 73 ± 33 s (63 ± 17 s and 53 ± 22 s) for the first (second and third) slice(s). The velocity amplitude is found to be 9.4 ± 13 km s^{-1} (11 ± 13 km s^{-1} and 8 ± 15 km s^{-1}). We note that significant brightening along the loop, quasi-periodic flows, and transverse oscillations occur almost at same time for curved slice 1. The large error bars in velocity is because of large errors in the amplitude measurement. Errors in the amplitude estimation is large because 1σ error bars in the x–t map columns are larger than the observed amplitude of the structure. Since we have aligned the data with sub-pixel accuracy, the amplitude observed is due to the displacement of structure along the slit and not due to shifts and jitter (Morton & McLaughlin 2013, 2014). Therefore, we find evidence of short period, large velocity amplitude oscillations associated with braided magnetic structure.

4. CONCLUSION

In this study we investigate the high frequency dynamics of braided magnetic region as seen from Hi-C. Our filtered images reveal finer structures in contrast to the original images. These filtered images allow us to focus on the braided region and identify the threads within them. We produce power maps for periods in the 30–60 s interval and find that such periodicities are present in small spatial scales and can be detected with high temporal and spatial resolution only. Furthermore, the power maps reveal the finer structuring within the moss region. We find that significant power is present in the active moss and braided region as revealed by Hi-C. One can conjecture that high frequency power, if they are due to waves, are very much localized in the magnetic structures and are probably using them as wave guides for propagation. They seem to be restricted within these structures only. Testa et al. (2013) reported that the intensity variation in the moss region is due to coronal nanoflares and estimated its timescale to be ~15–20 s. In this study wavelet analysis reveals that shorter periodicities (~15–30 s) do exist but they are within the 95% significance level for a white noise process. Therefore, we cannot distinguish white noise with periodic signal variation. We find periodic intensity variation with time period of 30–60 s above the significance level, which could be due to recurrent plasma outflows associated with repeated magnetic reconnection in these regions or due to magnetoacoustic waves propagating along these fine structures, which can generate periodic variations in intensity. It is worthwhile to note that we cannot distinguish between flows or waves without spectroscopic observations. Therefore, in this study by flow, we mean apparent motion in the plane of sky.

Braided magnetic region as shown in Figure 1(f) is known to manifest a sufficient amount of magnetic free energy to heat the corona and to explain the observed brightening (Thalmann et al. 2014). Tiwari et al. (2014) reported subflares occurring in this region by analyzing the intensity in AIA images. They showed that such subflares are the consequences of magnetic reconnection. Cirtain et al. (2013) reported outflow velocities, driven by plasma pressure along the field as the plasma is heated locally, to be 100–150 km s^{-1} in this region because of free energy released during magnetic field dissipation due to reconnection. We have focused our attention on a highly probable reconnection site (see Tiwari et al. 2014). We find that the reconnections occurring in this region can drive plasma to a wide range of velocities from 13–185 km s^{-1}projected in the plane of sky depending on the strength of reconnection. Outflow velocities for most of them are lower than the sound speed (100 km s^{-1} for 1 MK plasma) while some of them are greater than sound speed.

Morton & McLaughlin (2013, 2014) reported the period of transverse oscillations in the moss region peaks at around 50 s, displacement around 40 km, and velocity amplitude peaking around 3 km s^{-1}. In this study we focused on short period and large amplitude oscillation and find that short period and large velocity amplitude oscillations are associated with the braided magnetic region where reconnection happens (Thalmann et al. 2014). McIntosh et al. (2011) reported the velocity amplitude of 5 ± 5 km s^{-1} using Monte-Carlo simulation in the active region of the Sun at coronal heights. Such low frequency waves are not energetic enough to heat the active corona. They have conjectured the presence of shorter period waves in the active region which cannot be resolved by SDO/AIA. Our analysis confirms the presence of large amplitude (~8–11 km s^{-1}) high frequency (~53–73 s) transverse waves in the braided magnetic region. The amplitude of these oscillations is ~67–110 km which is far below the spatial resolution limit of AIA. Therefore, such oscillations cannot be resolved by AIA. Such waves could be responsible for heating the active corona. Since significant brightening and plasma outflows observed in the braided magnetic region and transverse oscillation happen at same time, it is not yet clear whether reconnection drives the transverse waves or if transverse waves cause magnetic field lines to reconnect. Further studies are required to confirm this. Our results confirms the necessity of high temporal and spatial resolution combined imaging with spectroscopy for future missions.

We acknowledge the High resolution Coronal imager instrument team for making the flight data publicly available. MSFC/NASA led the mission and partners include the Smithsonian Astrophysical Observatory in Cambridge, MA;

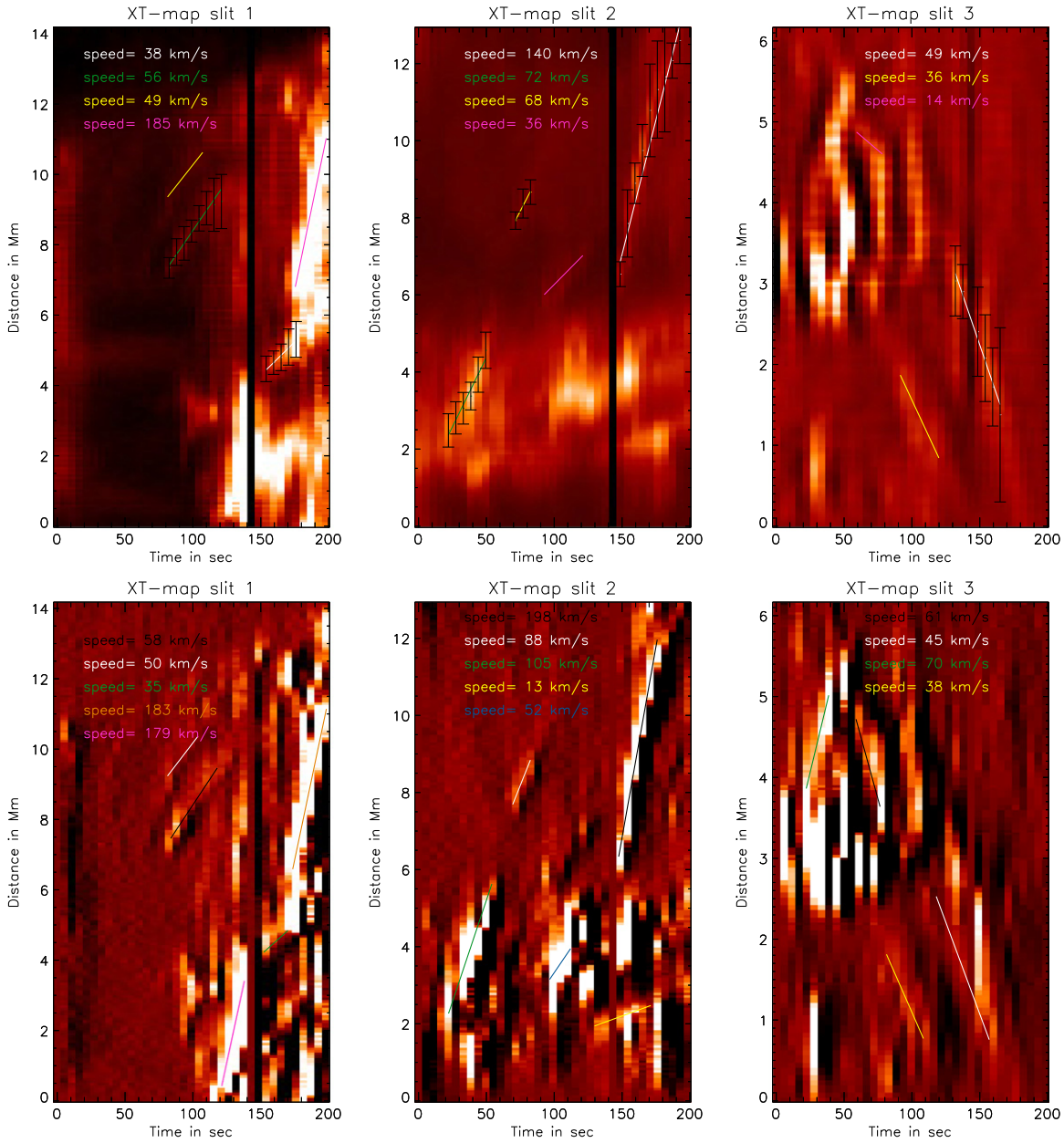

Figure 4. Top panel: time–distance (x–t) maps corresponding to the three curved slices marked as 1, 2, and 3 in Figure 1(e) overplotted with best fitting straight lines on the observed ridges. The slopes of the fitted lines providing an estimate of the speeds are also printed. The black vertical strip represents the data gap of one frame. Bottom panel: time–distance (x–t) maps of the running difference images corresponding to x–t maps in top panel.

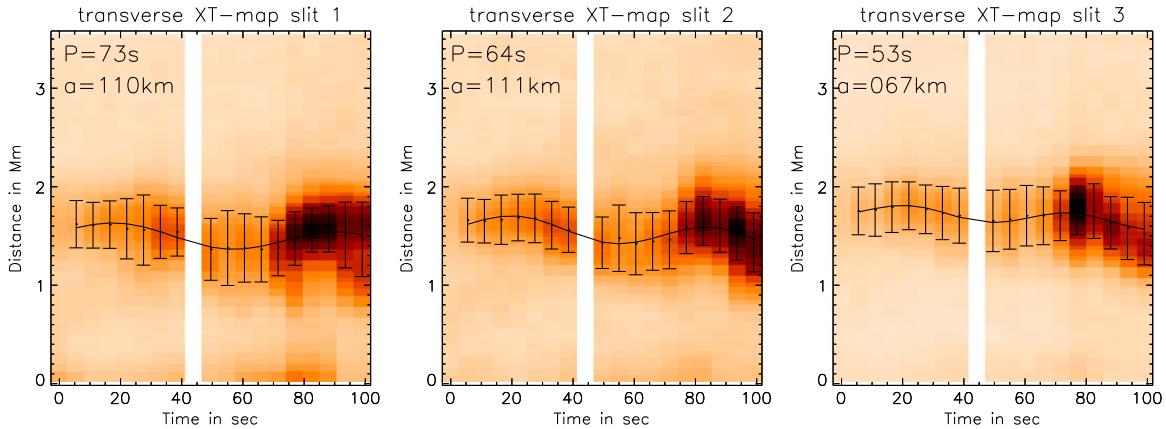

Figure 5. Inverted intensity x–t maps corresponding to the transverse slices marked as 1, 2, and 3 in Figure 1(f) overplotted with best fit sine curves. P and a are the time period and amplitude of oscillations. The white vertical strip represents the data gap of one frame.

Lockheed Martin Solar Astrophysical Laboratory in Palo Alto, CA; the University of Central Lancashire in Lancashire, UK; and the Lebedev Physical Institute of the Russian Academy of Sciences in Moscow.

REFERENCES

Antiochos, S. K., Karpen, J. T., DeLuca, E. E., Golub, L., & Hamilton, P. 2003, ApJ, 590, 547
Brooks, D. H., & Warren, H. P. 2009, ApJL, 703, L10
Cirtain, J. W., Golub, L., Winebarger, A. R., et al. 2013, Natur, 493, 501
Kobayashi, K., Cirtain, J., et al. 2014, SoPh, 289, 4393
McIntosh, S. W., de Pontieu, B., et al. 2011, Natur, 475, 477
Morton, R. J., & McLaughlin, J. A. 2013, A&A, 553, L10
Morton, R. J., & McLaughlin, J. A. 2014, ApJ, 789, 105
Morgan, H., & Druckmüller, M. 2014, SoPh, 289, 2945
Parker, E. N. 1988, ApJ, 330, 474
Peter, H., Bingert, S., Klimchuk, J. A., et al. 2013, A&A, 556, A104
Régnier, S., Alexander, C. E., Walsh, R. W., et al. 2014, ApJ, 784, 134
Testa, P., De Pontieu, B., Martínez-Sykora, J., et al. 2013, ApJL, 770, L1
Thalmann, J. K., Tiwari, S. K., & Wiegelmann, T. 2014, ApJ, 780, 102
Tiwari, S. K., Alexander, C. E., Winebarger, A. R., & Moore, R. L. 2014, ApJL, 795, L24
Tomczyk, S., McIntosh, S. W., Keil, S. L., et al. 2007, Sci, 317, 1192
Torrence, C., & Compo, G. P. 1998, BAMS, 61
Winebarger, A. R., Cirtain, J., Golub, L., & DeLuca, E. 2014, ApJ, 787, 10
Winebarger, A. R., Walsh, R. W., Moore, R., et al. 2013, ApJ, 771, 21
Yuan, D., & Nakariakov, V. 2012, A&A, 543, A9